Journal of Materials Chemistry B

Accepted Manuscript

ROYAL SOCIETY OF CHEMISTRY

www.rsc.org/materialsB

Multifunctional hydroxyapatite nanoparticle-based affinity adsorbent with sensing and fluorescence imaging capacity

Shasha Yao,[a] Yu Zhang,[a] Junli Zhang,[b] Xu Zhang,[a] Binjie Li,[ac] Yanbao Zhao*[a]

a .Key Laboratory for Special Functional Materials, Henan University, Kaifeng 475004, P. R. China

b. Key Laboratory of Plant Stress Biology, Henan University, Kaifeng 475004, P. R. China

c. Medical School of Henan University, Kaifeng 475004, P. R. China

Abstract

Nickel hydroxide/hydroxyapatite ($Ni(OH)_2$/HAP) nanoparticles (NPs) coated with rhodanmine B hydrazide (RBH) were successfully synthesized by three steps. First, $Ni(OH)_2$/HAP-COOH NPs were synthesized by a facile hydrothermal route in the presence of citric acid; Second, rhodamine B reacted with hydrazine hydrate to get rhodanmine B hydrazide (RBH); Last, RBH was conjugated on the surface of $Ni(OH)_2$/HAP-COOH NPs to form $Ni(OH)_2$/HAP-RBH. As affinity adsorbent, these NPs can directly purify histidine-tagged (His-tagged) proteins from the mixture of lysed cells, and present high protein adsorption capacity, with the maximum value of 115 mg/g. A prominent fluorescence enhancement at 578 nm was observed in the presence of Pt^{2+}, accompanied by the change in the absorption spectrum. These NPs display excellent selectivity and sensitive recognition toward Pt^{2+} over other metal ions and anions with a detection limit of 0.03 μM. These NPs present low cytotoxicity and can be used as a probe for Pt^{2+} and living cell imaging.

1. Introduction

Inorganic NPs have great importance in basic and applied research. In general, they have been functionalized with peptides, antibodies, and other molecules and used in biosensing, cellular imaging, drug delivery and separation.[1,2] Leduc et al. developed a novel gold nanoprobe that can be used for live-cell single-molecule imaging.[3] Magnetic mesoporous silica spheres were used as potential vectors for drug targeting and controlled-release systems.[4] Recently, many researchers

* Corresponding author. Tel.: +8637123881358; fax: +8637123881358

E-mail address: zhaoyb902@henu.edu.cn

are attempting to prepare multifunctional NPs, which would provide improving functionality and the synergistic effect between multiple components.[5,6] For example, the gold NPs surface-functionalized with PEG, biotin receptor, paclitaxel (PTX) and rhodamine B linked beta-cyclodextrin (β-CD) can be useful as a theranostic agent for cancer therapy.[7] The multifunctional silica nanospheres with Fe_3O_4 nanocrystals at the centre and a QD-layer at radial equidistance near the surface would be a promising platform for on-site biosensors.[8] Especially, affinity particle-adsorbents based on specific interactions between immobilized ligands and affinity tags on the protein have emerged as a promising nano-tool for the separation of proteins, which is easily adaptable to any protein expression system.[9-12] Multifunctional magnetic mesoporous core/shell heteronanostructure combines the capacity of effective protein purification from protein mixture and selective low molecule weight (MW) biomolecule enrichment.[13] Fluorophore-doped nickel chelate surface-modified silica NPs that functions in a dual mode, combining His-tagged protein purification with site-specific fluorophore labeling.[14] However, the preparation of multifunctional NPs has been challenging.

Hydroxyapatite ($Ca_{10}(PO_4)_6(OH)_2$, HAP) is the main inorganic component of hard tissues like bone and dental reparation and also for the applications in drug delivery systems and affinity adsorbents.[15,16] In particular, HAP has rich surface active groups and can be easily functionalized by conjugating ligands or other components.[17,18] The HAP-containing microspheres showed outstanding features with respect to *in vitro* calcification, high protein loading/controlled release, and cytocompatibility.[19,20] In addition, cisplatin and its analogues are widely used as anticancer drugs, it greatly promotes the development of medical treatment.[21,22] Despite the medical benefits of platinum compounds, other forms of platinum are considered potential health hazards.[23] Platinum salts can cause DNA alterations, cancers, autoimmune disorders, respiratory and hearing problems, and damages to organs. In this study, we designed and prepared a novel multifunctional HAP NP-based affinity adsorbent, which provides a convenient means of purifying His-tagged proteins. In addition, these NPs display excellent selectivity and sensitive recognition toward Pt^{2+} by fluorescence enhancement, and would be used as a probe for Pt^{2+} and living cell imaging.

2. Experimental section

2.1 Materials

Ammonium hydrogen phosphate ($(NH_4)_2HPO_4$), nickelous chloride ($NiCl_2·6H_2O$, ≥98.0%), calcium nitrate ($Ca(NO_3)_2·4H_2O$, ≥99.0%) and absolute alcohol were purchased from Tianjin Kermel Chemical Reagent Co., China. Ammonia solution ($NH_3·H_2O$, ≥25%) were from Luoyang Haohua Chemical Reagent Co. Ltd. Rhodamine B was purchased from Beijing chemical plant. 3-(4,5-dimethylthia-zol)-2,5-diphenyltetrazoliumbromide (MTT) and dimethylsulfoxide (DMSO) were purchased from Sigma (St. Louis, MO, USA). Hydrazine hydrate (80%) was purchased from Tianjin reagent plant. All chemical agents used in these experiments were of analytical grade and used directly without further purification. RPMI1640 and fetal calf serum (FCS) were purchased from Gibco (Grand Island, NY, USA). The solution of metal ions was prepared from their nitrate salts and chloride salts. Ni-NTA agarose, was from QIAGEN (Beijing, China). Protein molecular weight marker (Low) was purchased from TakaRa Biotech (Dalian, China).

2.2. Synthesis of $Ni(OH)_2$/HAP-RBH NPs

Preparation of $Ni(OH)_2$/HAP-COOH, 1.58 g $(NH_4)_2HPO_4$ and 0.1 g citric acid were dissolved in 100 mL distilled water, and 4.72 g $Ca(NO_3)_2·4H_2O$ and 1.19 g $NiCl_2·4H_2O$ were dissolved in 100 mL distilled water. Then, $(NH_4)_2HPO_4$ solution was added slowly into the $Ca(NO_3)_2$ solution and the pH value of the solution was tuned to 10. After reaction for 0.5 h, the solution was transferred into a Teflon-lined stainless-steel autoclave, sealed and heated at 165 ^oC for 12 h. Finally, the solution was cooled, centrifuged and washed to get $Ni(OH)_2$/HAP-COOH product.

RBH was synthesized according to the literature.[24] In a typical synthesis, 1.20 g rhodamine B was dissolved in 30 mL ethanol. Then 2 mL hydrazine hydrate was added to it. After the addition, the stirred mixture was heated to reflux for 2 h. The solution changed from purple to orange. Subsequently, the mixture was cooled and centrifuged. Last, 50 mL (1 M) HCl was added to the solid to generate a clear red solution. After that, the pH of the solution was slowly tuned to 9. The precipitate was centrifuged and washed to get RBH.

Preparation of $Ni(OH)_2$/HAP-RBH NPs**,** 70 mg $Ni(OH)_2$/HAP-COOH NPs was dispersed in 10 mL distilled water and 40 mg RBH was dissolved in 10 mL PBS buffer solution. Then $Ni(OH)_2$/HAP-COOH suspension was added dropwise into the RBH solution at 60 ^oC and held for 4 h under agitation. Last, the solution was cooled, centrifuged and washed to get target sample.

2.3 Analytical procedure

To 10 mL flasks, Pt^{2+} stock solution (1.0 mM, 0-100 μL), foreign ions (1.0 mM, 100 μL) and $Ni(OH)_2$/HAP-RBH solution (1 mg/mL, 100 μL) were respectively diluted to 10 mL using water. The solutions were shaken at a rotation speed of 120 rpm at room temperature for 30 min. After that, 3.0 mL of each solution was transferred to a 1 cm plant guard cell and the fluorescence measurement was carried out by excitation/emission at 530/578 nm.

2.4 Preparation and separation of His-tagged proteins

In this study, three different His-tagged proteins were prepared: His-tagged ASCORBATE PEROXIDASE3 (His-tagged APX3),[25] His-tagged calcium protein kinases (His-tagged CPK4)[26] and His-tagged thioredoxin 9 (His-tagged TRX9).[27] We cloned APX3 and CPK4 from *Arabidopsis thaliana* and constructed them into the pET-28a plasmid. His-tagged TRX9 was from PET-32a plasmid.[28] His-tagged recombinant plasmids were transformed into *E. coli* strain Rosetta (DE3) (Novagen) for protein expression using standard protocols.[29] The *E. coli* cells are lysed by 20 mM Tris (including 150 mM NaCl, pH = 8).

Theoretically, all the proteins with 6×His-tagged should be captured by metal-chelate affinity separation method. After being washed three times with Tris buffer, $Ni(OH)_2$/HAP-RBH NPs were added directly into 2 mL mixture of cell lysate and shaken for 40 min at a rotation speed of 90 rpm at room temperature. Then, the $Ni(OH)_2$/HAP-RBH NPs having captured His-tagged proteins were isolated from the solution by centrifugation and washed three times with Tris buffer in order to remove any residual uncaptured proteins. And then, the targeting NPs were washed with 300 μL imidazole solution (1.0 M) to disassociate His-tagged proteins from their surface. Separately collected protein solutions were detected by SDS-PAGE.

2.5 MTT test

The colorimetric MTT test was used to assess cell metabolic activity on the basis of the ability of the mitochondrial succinate-tetrazolium reductase system to convert the yellow dye MTT to a blue-colored formazan, and the cell viability is proportional to the color density formed. Human hepatoma cell line Bel-7402 were supplemented with 1 mM glutamine and 10 (v/v) FCS

respectively, and cultured at 37 °C under 5% CO_2 atmosphere. 1 mM amino guanidine was added as an inhibitor of amine oxidase derived from FCS and had no effect on the various parameters of the cells measured in this study.[33] After cells were seeded into 96-well plates at 5,000 cells/well for 24 h, $Ni(OH)_2$/HAP-RBH (0.02, 0.1, 0.2, 0.6 and 1 mg/L) were subsequently added and incubated for another 48 h, then, MTT stock solution (5 mg/mL) was added to each well followed by incubation for 4 h at 37 °C. The supernatant was then removed and cells were lysed with 100 μL DMSO. Absorbance was recorded at 570 nm using a power wave XS (BioTek).

2.6 Characterization

The morphology and composition were characterized by transmission electron microscopy (TEM, JSM-5600 V, Japan), fourier transform infrared (FT-IR, AVATAR360, America), X-ray diffraction (XRD, X-Pertpro, Holland), fluorescence spectrometer (FL, FluoroSENS, Britain), ultraviolet-visible absorption spectroscopy (PE-Lambda 35, America) and thermogravimetric analysis (TG, EXSTAR 6000), respectively. The separated His-tagged proteins were detected with sodium dodecylsulfate polyacrylamide gel electrophoresis (SDS-PAGE, Power PAC 300, China), with the preconcentration voltage of 70 V and the separation voltage of 120 V. The binding proteins concentration was analyzed by BCA protein assay kit, and BSA was a standard sample to make a standard curve.

3. Results and discussion

Fig. 1a gives the TEM images of the obtained $Ni(OH)_2$/HAP-COOH NPs. The obtained $Ni(OH)_2$/HAP-COOH sample is in nanorod shape and its average size is 40 nm × 10 nm. It can be clear that $Ni(OH)_2$/HAP-RBH is similar to that of $Ni(OH)_2$/HAP-COOH, and RBH modification does not affect the morphology feature (Fig. 1b). Fig. 1c shows the number distribution of $Ni(OH)_2$/HAP-COOH and $Ni(OH)_2$/HAP-RBH NPs. Their size distribution curve presents single peak (51 nm / 58 nm) and the polydispersity index (PDI) is respectively 0.388 and 0.645, which is close to the TEM observation, indicating that the obtained NPs are dispersed. The XRD pattern of $Ni(OH)_2$/HAP-RBH displays multiple diffraction peaks and these peaks correspond to crystalline HAP (JCPDS 09-0432) and nickel hydroxide (JCPDS 14-0117), respectively, which indicates the formation of $Ni(OH)_2$/HAP-COOH composite (Fig. 1d).

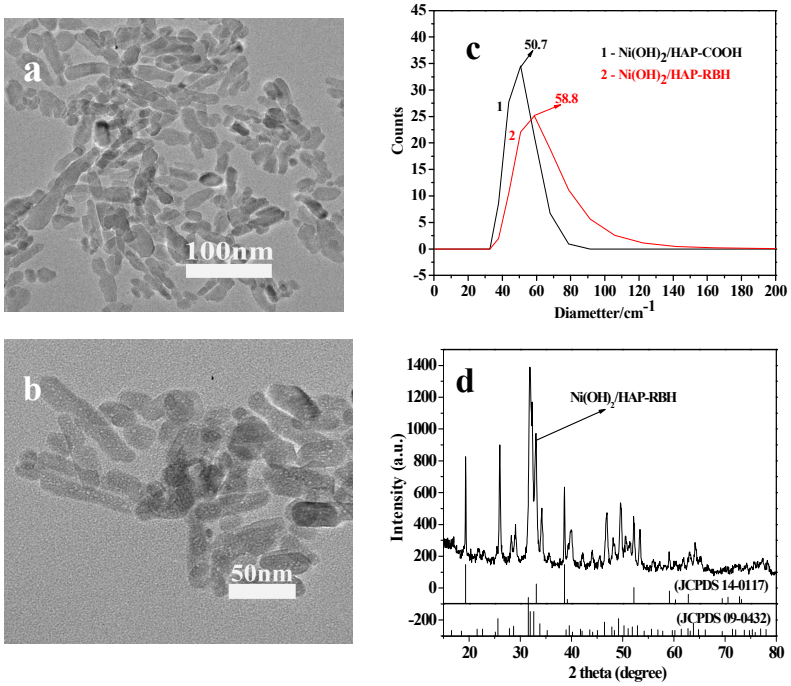

Fig. 1 TEM image of $Ni(OH)_2$/HAP-COOH (a) and $Ni(OH)_2$/HAP-RBH NPs (b), size distribution of $Ni(OH)_2$/HAP-COOH and $Ni(OH)_2$/HAP-RBH NPs (c) and XRD pattern (d) of $Ni(OH)_2$/HAP-RBH NPs.

Fig. 2a displays the FT-IR spectrum of the prepared $Ni(OH)_2$/HAP-RBH NPs. There appears a broad band observed around 3435 cm^{-1}, which is assigned to the stretching vibrations of hydroxyl group. The adsorption peaks at 1039 and 570 cm^{-1} were characteristic of P–O bonds in PO_4^{3-} group.[30] The bands at 1695 cm^{-1} ascribed to the characteristic of carbonyl adsorption.[31] In addition, the characteristic adsorption of RBH at 1689 cm^{-1} can be observed in $Ni(OH)_2$/HAP-RBH NPs,[24] indicating that RBH was conjugated on the surface of Ni(OH)2/HAP-COOH NPs. Fig. 2b gives TG analyses of $Ni(OH)_2$/HAP-RBH NPs samples. For Ni(OH)2/HAP-COOH sample, there appears a successive mass loss process from room temperature to 800 ^oC. The initial mass loss below 100 ^oC can be attributed to desorption of adsorbed water and the following mass loss (250-320 ^oC) is related to releasing citric acid or crystal water (total mass loss 5 %). For $Ni(OH)_2$/HAP-RBH NPs, the main mass loss in the range of 250 ^oC and 400 ^oC is due to decomposition of RBH, which indicates that RBH is coating on the surface of $Ni(OH)_2$/HAP-COOH NPs.

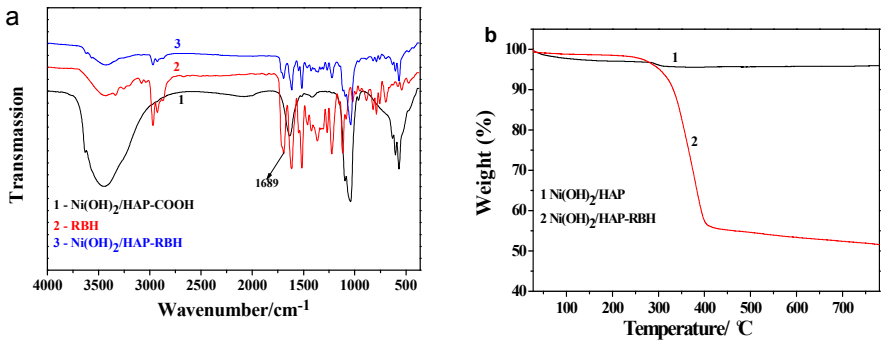

Fig. 2 FTIR spectra (a) and TG (b) of the prepared $Ni(OH)_2$/HAP-RBH NPs.

$Ni(OH)_2$/HAP-RBH NPs can be used for direct separation of His-tagged proteins from crude cell lysate. Here, the total TRX9 protein in crude cell lysate was 1.83 g/L determined by BCA protein assay kit, and 10 mg $Ni(OH)_2$/HAP-RBH NPs could adsorb 1.41 g/L (recovery percentage is 77%) from 10 mL cell lysate, which was close to that of commercial microbeads (10 mg, 1.49 g/L, 81%). Fig. 3 gives SDS-PAGE analysis of the purified His-tagged TRX9 proteins. Lane M is molecular weight markers and lane L is *E. coli* cell lysate. The MW of His-tagged TRX9 was 14.3 KD. With the extension of adsorption time, the amount of His-tagged proteins-bound to $Ni(OH)_2$/HAP-RBH increases gradually. When adsorption time is 10 min, 20 min, 30 min, 40 min, 1 hr and 2 hr, the binding capacity is 14.7 mg/g, 28.3 mg/g, 48 mg/g, 51 mg/g, 56.7 mg/g and 58.7 mg/g, respectively (Fig. 3a lane 1 - 6). When the adsorption time is 40 min, the binding capacity achieves a balance. In addition, the amount of His-tagged TRX9 washed off from $Ni(OH)_2$/HAP-RBH NPs was increased with increasing concentration of imidazole in the range of 0.1 M to 2.0 M (Fig. 3b 1 - 4), and the maximum value was 115 mg/g.

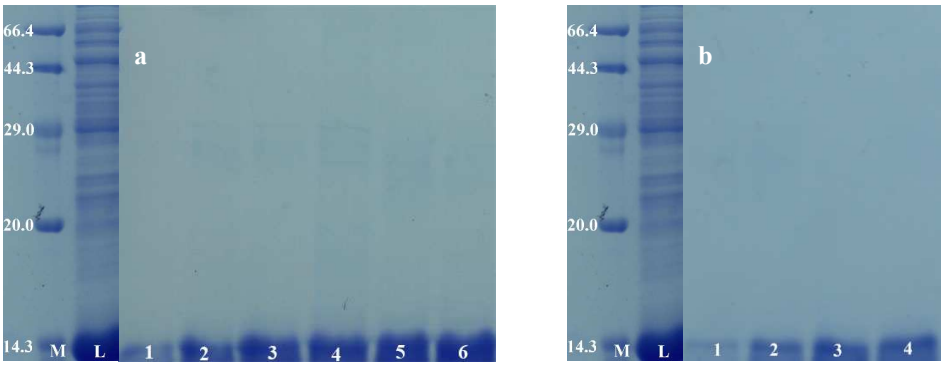

Fig. 3 SDS-PAGE analysis of purified recombinant protein by synthesized NPs. Lane L TRX9 *E. coli* lysate. Lane M Marker. (a) Lane 1 - 6, the fractions washed off from the $Ni(OH)_2$/HAP-RBH NPs when different adsorption time were used (lane 1, 10 min; lane 2, 20 min; lane 3, 30 min, lane 4, 40 min; lane 5, 1 hr; lane 6, 2 hr). (b) Lane 1 – 4, the fractions washed off from the $Ni(OH)_2$/HAP-RBH NPs with different amount of imidazole (lane 1, 0.1 M; lane 2, 0.5 M; lane 3, 1 M; lane 4, 2 M).

To ensure the detection limit of the $Ni(OH)_2$/HAP-RBH NPs for separating target proteins, the His-tagged TRX9 proteins with different concentrations were employed (Fig. 4a lane 1 - 4). It is clear that the quantity of proteins captured by $Ni(OH)_2$/HAP-RBH NPs depended directly on the concentration of proteins in cell lysate. In the test concentration range, the $Ni(OH)_2$/HAP-RBH NPs displayed negligible nonspecific protein adsorption. When TRX9 proteins were 1.0×10^{-4} M, 5.0×10^{-5} M, 1.0×10^{-5} M, 5.0×10^{-6} M, 2.0×10^{-6} M, 1.0×10^{-6} M, and 8.0×10^{-7} M, the binding capacity of $Ni(OH)_2$/HAP-RBH NPs (5 mg) were 79.7 mg/g, 62.7 mg/g, 56 mg/g and 28.7 mg/g, 19 mg/g, 14 mg/g, 9.5 mg/g, respectively. By coupling with facile SDS-PAGE, the $Ni(OH)_2$/HAP-RBH NPs can be used to detect target proteins at a detection limit of 8.0×10^{-7} M.

The universality of $Ni(OH)_2$/HAP-RBH NPs was evaluated by separating three kinds of His-tagged proteins (His-tagged TRX9, His-tagged APX3 and His-tagged CPK4) from the *E. coli* lysate solution. Their MW was 14 kDa, 30 kDa and 58 kDa, respectively. Fig. 4b gives the SDS-PAGE analysis of purified recombinant proteins. It can be seen that three kinds of recombinant proteins can be separated specifically from the *coli* lysate. The binding capacity of $Ni(OH)_2$/HAP-RBH NPs (5 mg) was 61 mg/g (TRX9), 8.7 mg/g (CPK4) and 21.3 mg/g (APX3), respectively. It is clear that the $Ni(OH)_2$/HAP-RBH NPs display higher binding properties and specificity, and are suitable for low molecule weight proteins.

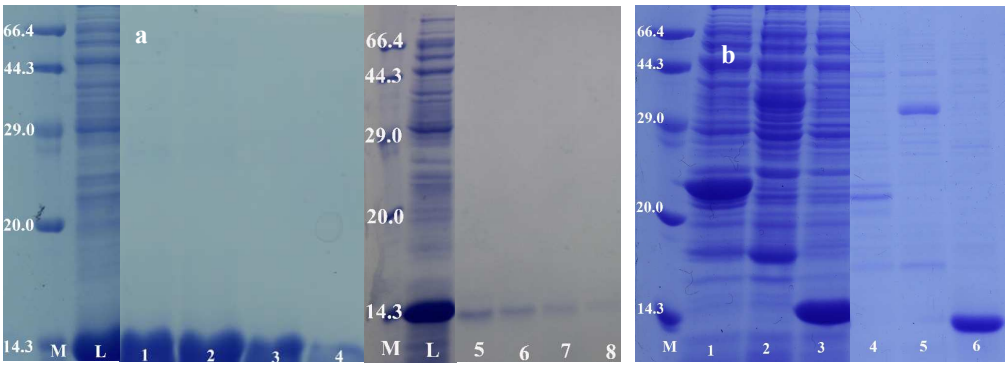

Fig. 4 SDS-PAGE analysis of purified His-tagged proteins. (a) Lane L TRX9 *E. coli* lysate. Lane M Marker. Lane 1-4, the fraction washed off from $Ni(OH)_2$/HAP-RBH NPs when different concentration of His-tagged TRX9 proteins were used (lane 1, 1.0×10^{-4} M; lane 2, 5.0×10^{-5} M; lane 3, 1.0×10^{-5} M; lane 4, 5.0×10^{-6} M; lane 5, 5.0×10^{-6} M; lane 6, 2.0×10^{-6} M; lane 7, 1.0×10^{-6} M; lane 8, 8.0×10^{-7} M;). (b) lane 1, His-tagged APX3 *E. coli* lysate; lane 2, His-tagged CPK4 *E. coli* lysate; lane 3, His-tagged TRX9 *E. coli* lysate; lane 4-6, the fractions washed off from the $Ni(OH)_2$/HAP-RBH NPs when different kinds of His-tagged proteins were used (lane 4, His-tagged APX3; lane 5, His-tagged CPK4; lane 6, His-tagged TRX9).

The activity of His-tagged protein purified by $Ni(OH)_2$/HAP-RBH NPs was tested by thermal activation.[32] Fig. 5a shows the photos of His-tagged protein solution with three different conditions. The purified His-tagged protein solution is clear and transparent (sample a), while the denatured protein present flocculent precipitation (sample b) and the precipitation can be separated by centrifugation (sample c). It is clear that the His-tagged proteins separated by $Ni(OH)_2$/HAP-RBH NPs has high activity. Fig 5 b gives the cytotoxicity of $Ni(OH)_2$/HAP-RBH NPs to human hepatoma cell BEL-7402. It is clear that $Ni(OH)_2$/HAP-RBH NPs don't inhibit the cell growth in the range of 0.02 to 1 μg/mL, while promote cell growth at 0.6 μg/mL, indicating that these NPs present low cytotoxicity.

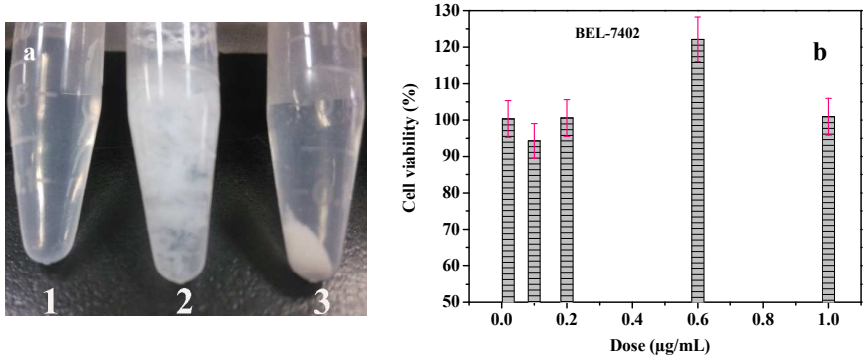

Fig. 5 (a) Results of heat shock experiments on His-tagged TRX9 proteins. (1) the His-tagged proteins solution purified by $Ni(OH)_2$/HAP-RBH NPs. (2) denaturated protein. (3) denatution protein after centrifugation. (b) The cytotoxicity of $Ni(OH)_2$/HAP-RBH NPs to human hepatoma cell BEL-7402.

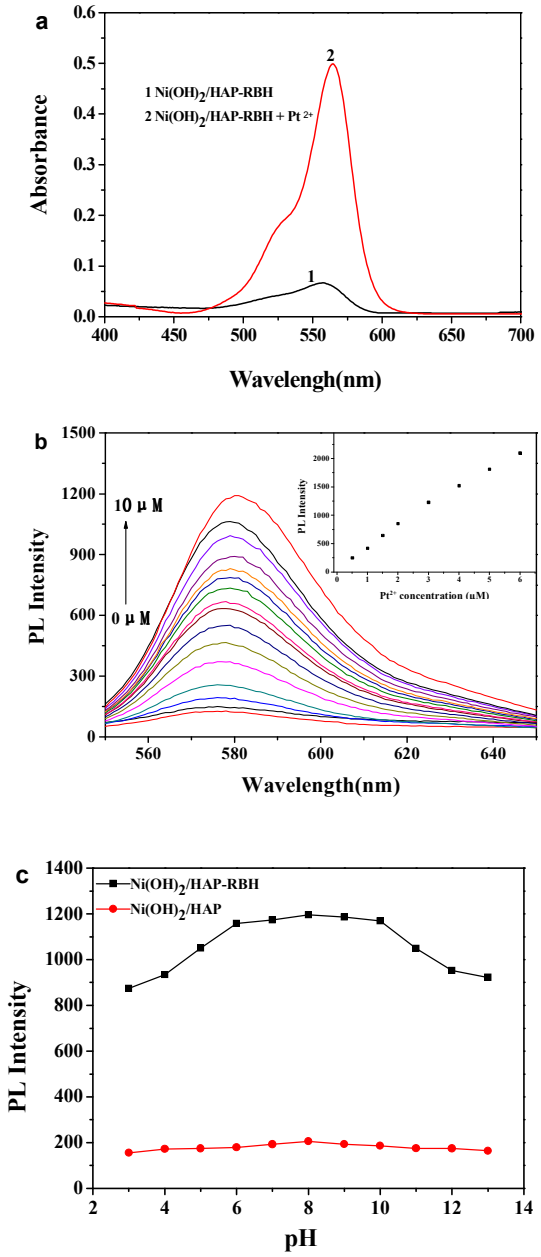

Fig. 6 (a) UV-vis absorbance of $Ni(OH)_2$/HAP-RBH (10 μg/mL) without and with Pt^{2+} (10 μM) in water. (b) Fluorescent spectra of $Ni(OH)_2$/HAP-RBH solution in the presence of different concentrations of Pt^{2+}(0-10 μM). λex = 530 nm. Inset: fluorescence intensity at 578 nm as a function of Pt^{2+} concentration. (c) Effect of pH on the reaction of Pt^{2+} (10 μM) with $Ni(OH)_2$/HAP-RBH (10 μg/mL) and only 10 μg/mL $Ni(OH)_2$/HAP-RBH NPs.

Fig. 6 shows UV-vis absorption and fluorescence spectra of $Ni(OH)_2$/HAP-RBH NPs (10 μg/mL) dispersed in water. The absorption spectra of $Ni(OH)_2$/HAP-RBH exhibit a very weak band at about 556 nm. When Pt^{2+} is added into the solution, it can chelate with RBH conjugated

on NPs and induce ring-opening at C-N bond in spirolactam to generate a rhodamine-type intermediate with a strong absorption at 565 nm (Fig. 6a). It was also found that the addition of Pt^{2+} to $Ni(OH)_2$/HAP-RBH solution could cause a significant enhancement of fluorescence. With increasing Pt^{2+} concentrations, fluorescence intensity increased, and the fluorescent intensity at 578 nm was proportional to Pt^{2+} concentration over a range of 0-10 μM (Fig. 6b). A linear relationship for Pt^{2+} detection under the optimum conditions was obtained at 578 nm with a correlation coefficient of 0.9964. The regression equation is Y = 207.3210 + 31.1378X. Based on $3 \times \delta_{blank}/k$ (where δ_{blank} is the standard deviation of the blank solution and k is the slope of the calibration plot), the limit of detection for Pt^{2+} is up to 3.0×10^{-8} M (insert). In addition, the fluorescence presents obvious pH-dependence. In a pH range of 6.0-10.0, the stable and enhance fluorescence was obtained (Fig. 6c). Therefore, $Ni(OH)_2$/HAP-RBH NPs was favorable for its application in biological and medical samples, as most of such samples exist at neutral conditions.

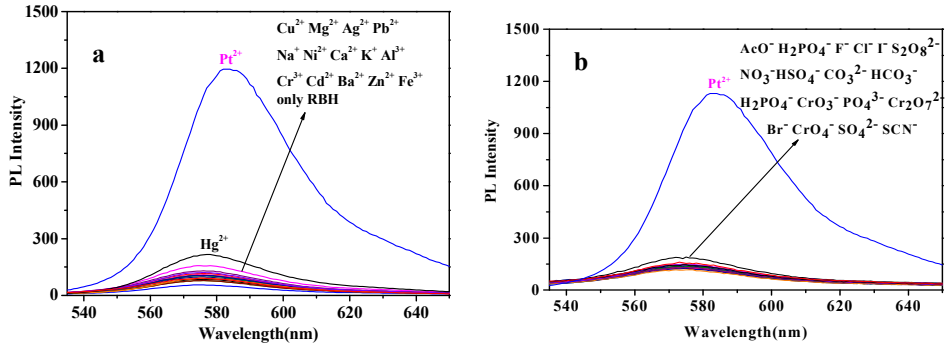

Fig. 7 Fluorescence intensity of $Ni(OH)_2$/HAP-RBH (10 μg/mL) in water with 10 μM metal ions and anions. (a): Cu^{2+}, Mg^{2+}, Ag^{+}, Pb^{2+}, Na^{+}, Ni^{2+}, Ca^{2+}, K^{+}, Al^{3+}, Cr^{2+}, Cd^{2+}, Ba^{2+}, Zn^{2+}, Fe^{3+} and only RBH; (b): AcO^{-}, F^{-}, Cl^{-}, I^{-}, $S_2O_8^{2-}$, NO_3^{-}, HSO_4^{-}, CO_3^{2-}, HCO_3^{-}, $H_2PO_4^{-}$, ClO_3^{-}, PO_4^{3-}, $Cr_2O_7^{2-}$, Br^{-}, CrO_4^{2-}, SO_4^{2-} and SCN^{-}, and λex= 530 nm.

Some metal ions and anions were used to analyze the selectivity of probe $Ni(OH)_2$/HAP-RBH NPs. Fig. 7 gives the fluorescence spectra of $Ni(OH)_2$/HAP-RBH NPs (10 μg/mL) with various metal ions and anions (10 μM). $Ni(OH)_2$/HAP-RBH NPs (10 μg/mL) in water showed a very weak fluorescence in the absence of metal ions. However, the addition of Pt^{2+} ion resulted in a remarkably enhanced fluorescence at 578 nm. Other metal ions, such as Ag^{+}, Pb^{2+}, Na^{+}, K^{+}, Cr^{3+}, Cd^{2+}, Ba^{2+}, Zn^{2+}, Mg^{2+}, Hg^{2+}, Cu^{2+}, Ni^{2+}, Ca^{2+}, Al^{3+}, Fe^{3+} and anions including

SCN^-, $SO4^{2-}$, CrO_4^{2-}, Br^-, $Cr_2O_7^{2-}$, PO_4^{3-}, ClO^{3-}, F^-, Cl^-, I^-,$S_2O_8^{2-}$, NO^{3-}, HSO_4^-, CO_3^{2-}, HCO_3^-, $H_2PO_4^-$ and CH_3COO^- display no obvious fluorescent enhancements under identical conditions. These results indicated that $Ni(OH)_2$/HAP-RBH NPs could selectively recognize Pt^{2+} in the presence of competitive metal ions and anions in water.

In order to examine the practical applicability of the probe in biological samples, fluorescence imaging experiments were conducted in living cells. The fluorescence images of cells were investigated before and after addition of Pt^{2+} (Fig. 8). Plant guard cells and human hepatoma cell line BEL-7402 were incubated with $Ni(OH)_2$/HAP-RBH (10 μg/mL) for 30 min at room temperature in PBS and an insignificant fluorescence was detected in the cells' interior (Fig. 8a, d). Upon addition of Pt^{2+} (0.1 mM), strong red fluorescence was detected in the live cells by fluorescence microscopy. The fluorescent changes of $Ni(OH)_2$/HAP-RBH were then assayed in live cells in the presence of Pt^{2+}. After incubation with Pt^{2+} and $Ni(OH)_2$/HAP-RBH, the treated cells were still alive (Fig. 8c, f). These results demonstrate the efficient Pt^{2+}-sensing capability of $Ni(OH)_2$/HAP-RBH in live cells.

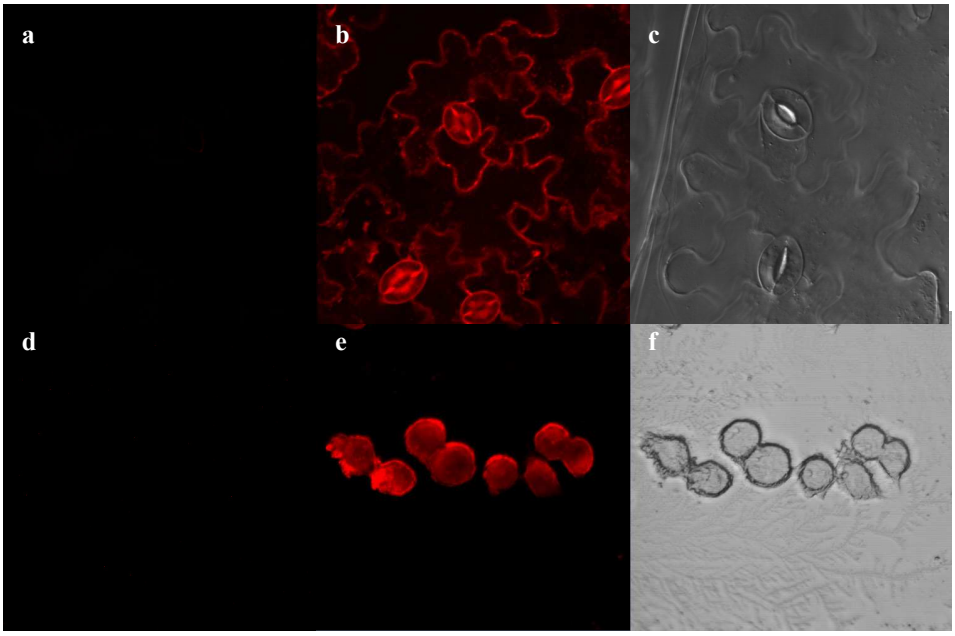

Fig. 8 Confocal fluorescence images of plant guard cells and human hepatoma cell line BEL-7402. (a, d) Cells incubated with 10 μg/mL $Ni(OH)_2$/HAP-RBH (a,d) in PBS buffer for 30 min; (b, e) Cells incubated with 10 μg/mL $Ni(OH)_2$/HAP-RBH and 10 μM Pt^{2+} in PBS buffer for 30 min (λex= 530 nm); (c, f) Brightfield image of cells shown in panel (b, e).

4. Conclusions

In this paper, we have designed and synthesized a novel multifunctional hydroxyapatite nanoparticle-based affinity adsorbent, $Ni(OH)_2$/HAP-RBH NPs, which can capture His-tagged proteins directly from the mixture of lysed cells. They have a high specificity and adsorption capacity, and are especially suitable for purification of His-tagged proteins. Upon addition of Pt^{2+}, this adsorbent exhibits remarkably enhanced fluorescent intensity, and excellent selectivity toward Pt^{2+} over other metal ions and anions. They can be also used as a probe for Pt^{2+} and living cell imaging.

Acknowledgement

Financial support of this work from National Natural Sceience Foundation of China (21271062), Foundation of Science and Technology of Henan Province (14B150003) and Program for Changjiang Scholars and Innovative Research Team (PCS IRT1126) are gratefully acknowledged.

References

1 X. Hu, M. Wang, F. Miao, J. Ma, H. Shen and N. Jia, *J. Mater. Chem. B*, 2014, 2, 2265–2275.

2 R. Li, L. Li, Y. Han, S. Gai, F. He and P. Yang, *J. Mater. Chem. B*, 2014, 2, 2127–2135.

3 C. Leduc, S. Si, J. Gautier, M. Soto-Ribeiro, B. Wehrle-Haller, A. Gautreau, G. Giannone, L. Cognet and B. Lounis, *Nano Lett.*, 2013, 13, 1489–1494.

4 S. Huang, Y. Fan, Z. Cheng, D. Kong, P. Yang, Z. Quan, C. Zhang and J. Lin, *J. Phys. Chem.*, *C* 2009, 113, 1775–1784.

5 B. Asadishad, M. Vossoughi and I. Alemzadeh, *Ind. Eng. Chem. Res.*, 2010, 49, 1958–1963.

6 M. F. Foda, L. Huang, F. Shao and H.-Y. Han, *ACS Appl. Mater. Interfaces*, 2014, 6, 2011−2017.

7 D. N. Heo, D. H. Yang, H.-J. Moon, J. B. Lee, M. S. Bae, S. C. Lee, W. J. Lee, I.-C. Sun, I. K. Kwon, *Biomaterials*, 2012, 33, 856–866.

8 W. Park, M. J. Kim, Y. Choe, S. K. Kim and K. Woo, *J. Mater. Chem. B*, 2014, 2, 1938–1944.

9 Y.-C. Lin, M.-R. Liang, Y.-C. Lin and C.-T. Chen, *Chem. Eur. J.*, 2011, 17, 13059–13067

10 X. Zou, K. Li, Y. Zhao, Y. Zhang, B. Li and C. Song, *J. Mater. Chem. B*, 2013, 1, 5108–5113

11 M. Shao, F. Ning, J. Zhao, M. Wei, D. G. Evans and X. Duan, *J. Am. Chem. Soc.*, 2012, 134, 1071−1077

12 J. Bao, W. Chen, T. Liu, Y. Zhu, P. Jin, L. Wang, J. Liu, Y. Wei and Y. Li. *ACS NANO*, 2007, 4, 293–298.

13 Z. Liu, M. Li, X. Yang, M. Yin, J. Ren and X. Qu, *Biomaterials*, 2011, 32, 4683–4690.

14 S. H. Kim, M. Jeyakumar and J. A. Katzenellenbogen, *J. Am. Chem. Soc.*, 2007, 129, 13254–13264.

15 J. Krenkova, N. A. Lacher and F. Svec, *Anal. Chem.*, 2010, 82, 8335–8341.

16 V. S. Chandra, G. Baskar, R. V. Suganthi, K. Elayaraja, M. I. A. Joshy, W. S. Beaula, R. Mythili, G. Venkatraman and S. N. Kalkura, *ACS Appl. Mater. Interfaces*, 2012, 4, 1200−1210.

17 S. Yao, Y. Huang, Y. Zhao, Y. Zhang, X. Zou and C. Song, *Mater. Sci. Eng. C*, 2014, 39, 1–5.

18 J. Lee and H.-S. Yun, *J. Mater. Chem. B*, 2014, 2, 1255–1263.

19 R. K. Singh, T.-H. Kim, K. D. Patel, J.-J. Kim and H.-W. Kim, *J. Mater. Chem. B*, 2014, 2, 2039–2050

20 X. Zhao, Y. Zhu, F. Chen, B.-Q. Lu, J. Wu, *CrystEngComm*, 2013, 15, 206–212.

21 A. V. Klein and T. W. Hambley. *Chem. Rev.*, 2009, *109,* 4911–4920.

22 P. Marqués-Gallego, H. den Dulk, J. Brouwer, S. Tanase, I. Mutikainen, U. Turpeinen and J. Reedijk. *Biochem. Pharmacol.*, 2009, 78, 365–373.

23 M. Ravera, E. Gabano, M. Sardi, G. Ermondi, G. Caron, M. J. McGlinchey, H. Müller-Bunz, E. Monti, M. B. Gariboldi and D. Osella, *J. Inorg. Biochem.*, 2011, 105, 400–409.

24 Y. Xiang, L. Mei, N. Li and A. Tong. *Anal. Chim. Acta*, 2007, 581, 132–136.

25 S.-Y. Zhu, X.-C. Yu, X.-J. Wang, R. Zhao, Y. Li, R.-C. Fan, Y. Shang, S.-Y. Du, X.-F. Wang, F.-Q. Wu, Y.-H. Xu, X.-Y. Zhang and D.-P. Zhang. *Plant Cell*, 2007, 19, 3019–3036.

26 S. Narendr, S. Venkataramani, G. Shen, J. Wang, V. Pasapul, Y. Lin, D. Kornyeyev, A. S. Holaday and H. Zhang. *J. Exp. Bot.*, 2006, 57, 3033–3042.

27 L. Meng, J. H. Wong, L. J. Feldman, P. G. Lemaux and B. B. Buchanan. *PNAS*, 2010, 107, 3900–3905.

28 E. R. LaVallie, A. Rehemtulla, L. A. Racie, E. A. DiBlasio, C. Ferenz, K. L. Grant, A. Light and J. M. McCoy. *J. Bio. Chem.*, 1993, 5, 23311–23317.

29 J. Sambrook and D. W. Russell, Molecular Cloning: a laboratory manual, Cold Spring Harbor Laboratory Press, New York, 2001, 1, 1252–1255.

30 Z. Boukha, M. Kacimi, M. F. R. Pereira, J. L. Faria, J. L. Figueiredo and M. Ziyad. *Appl. Catal. A*, 2007, 317, 299–309.

31 J. Zhang, Y. Zhou, W. Hu, L. Zhang, Q. Huang and T. Ma, *Sens. Actuator B*, 2013, 183, 290–296.

32 J. Chen and J. Chen, *J. Beijing Univ. Chem. Tech.*, 2006, 33, 34–37.

33 S. Xie, J. Wang, H. Ma, P. Cheng, J. Zhao and C .Wang, Toxicol., 2009, 263,127–133.